In-medium nuclear cluster energies within the extended Thomas-Fermi approach

François Aymard,[1] Francesca Gulminelli,[1] and Jérôme Margueron[2,3]
[1]*CNRS and ENSICAEN, UMR6534, LPC, 14050 Caen Cedex, France*
[2]*Institut de Physique Nucléaire de Lyon, Université Claude Bernard Lyon 1, F-69622 Villeurbanne Cedex, France*
[3]*IN2P3-CNRS, F-69622 Villeurbanne Cedex, France*
(Received 11 April 2014; published 30 June 2014)

A recently introduced analytical model for the nuclear density profile [P. Papakonstantinou, J. Margueron, F. Gulminelli, and Ad. R. Raduta, Phys. Rev. C **88**, 045805 (2013)] is implemented in the extended Thomas-Fermi energy density functional. This allows us to (i) shed a new light on the issue of the sign of surface symmetry energy in nuclear mass formulas, which is strongly related to the nonuniformity of the isospin asymmetry in finite nuclei, as well as to (ii) evaluate the in-medium corrections to the nuclear cluster energies in thermodynamic conditions relevant for the description of the (proto)neutron star crust. The ground-state configurations of the model are compared to Hartree-Fock calculations in spherical symmetry for some selected isotopic chains, and systematic errors are quantified. The in-medium modification of the nuclear mass due to the presence of a gas component is shown to strongly depend both on the density and the asymmetry of the nucleon gas. This shows the importance of accounting for such effects in the realistic modelizations of the equation of state for core-collapse supernovae and protoneutron stars.

DOI: 10.1103/PhysRevC.89.065807 PACS number(s): 26.60.Gj, 26.50.+x, 21.60.Jz, 21.65.Ef

I. INTRODUCTION

The semiclassical Thomas-Fermi (TF) and extended Thomas-Fermi (ETF) approach to the density-functional theory were largely used in the 1980s for nuclear structure applications [1–3] as well as astrophysical ones [4,5]. Two motivations of searching for approximations of the microscopic mean-field theory with effective interactions can be advanced. On one side, this semiclassical quasianalytical theory provides a clear physical insight on the functional dependence of nuclear energies and density profiles, which cannot be achieved with the numerical resolution of HF equations for single-particle orbitals. On the other side, the computational resources at that time made systematic HF calculations very hard to perform with reliable numerical error bars. The exponential progress of numerical computing in the next two decades made this motivation obsolete and we have assisted to an impressive progress of mean-field and beyond-mean-field large-scale nuclear structure calculations [6]. However in the recent years, a renewed interest towards the ETF theory has appeared [7–9]. This is largely due to the new challenges that are open to the field and the needs for a microscopic description of the very exotic nuclear species, which are expected to exist in stellar matter. The widely used equation-of-state models for supernova matter, neutron stars, and protoneutron stars typically replace the nuclear distribution in stellar matter with a single representative nucleus, and use density functionals to describe the nucleus as well as the surrounding nucleon gas [10,11]. More recent models have replaced the single nucleus approximation by a statistical distribution of nuclei, using the experimental information for nuclear masses and, in doing so, do not consider in-medium modifications to the nuclear cluster energies [12–15]. A complete and microscopic description of stellar matter at finite temperature and at subsaturation densities implies the evaluation of an extremely large database of ground states and excited nuclear configurations in a dilute light-particles environment, which are not directly accessible to variational HF calculations, or, for some of them that are accessible, which are computationally too expensive for large-scale calculations [16].

In this context it is interesting to develop an ETF-based formalism that would, in a quasianalytical way, provide nuclear clusters energies for ground-state and excited-state configurations using energy functionals optimized for exotic nuclear data as well as neutron matter calculations [17]. In a recent paper [18], we have proposed a model based on a simple parametrization of Fermi-Dirac density profiles and on the zeroth-order TF approximation for the kinetic energies and currents.

Comparing this model to HF ground-state configurations, a good agreement was reached since the differences between the model and the HF calculation were found independent of the gas density and of the order of 0.5–1 MeV/nucleon. The model has therefore been employed to evaluate the in-medium energy shifts in a large variety of excited-state configurations [18,19].

In this paper we introduce second-order $\hbar^2$ corrections, allowing the introduction of the spin-orbit interaction and an increased precision in the evaluation of the kinetic energy density. The agreement with HF energies is therefore found to be better. This improved model is used to obtain the functional form of the nuclear energies as a function of mass number and asymmetry, both in the case of ordinary nuclei in the vacuum, and in the case of nuclei immersed in a nucleon gas.

The paper is organized as follows: In Sec. II we recall the ETF formalism and present two possible modelings of the nuclear density profiles employed in the variational ETF. These two parametrizations are critically compared in Sec. III, which presents a comparison of the ETF model to HF calculations in order to assess the accuracy of the ETF calculation. It is shown that the inclusion of second-order $\hbar^2$ terms considerably improves the predictive power of the model. Section IV presents an application of the model to the

study of the functional dependence of the symmetry energy on the nuclear mass. We analyze the well known problem of the sign of the surface symmetry energy [20], and show that an explicit comparison to HF calculations can help to eliminate the ambiguity in the decomposition between surface and bulk in the two-component nuclear system. Section V reports detailed results concerning the modification to the nuclear energy due to the presence of a gas component. The specific case of a nucleus immersed in a neutron gas, similar to the ground state of nuclear clusters present in the crust of neutron stars, is examined. The case where the nucleus is in an arbitrary single-particle excited-state configuration, as it is the case in the finite temperature conditions of supernova matter and protoneutron stars, is also considered and shown to lead to very different energy shifts.

II. MODEL

We briefly present the model for nuclei and nuclear matter, which is based on the Skyrme interaction [17] and where the semiclassical ETF approximation is employed. This approximation requires a parametrization of the nuclear density profiles and two types of such parametrizations are investigated and compared.

A. Skyrme functionals and ETF semiclassical approximation

The Skyrme functional for the time-even energy density is expressed as [21,22]

$$\mathcal{E}_{\rm sky}(r) = \frac{\hbar^2}{2m}\tau^{(0)} + \sum_{t=0,1} C_t^{\rho}(\rho^{(0)})\rho^{(t)2} + C_t^{\Delta\rho}\rho^{(t)}\Delta\rho^{(t)} + C_t^{\tau}\rho^{(t)}\tau^{(t)} + \frac{1}{2}C_t^{J}J^{(t)2} + C_t^{\nabla J}\rho^{(t)}\nabla\cdot J^{(t)}, \quad (1)$$

where the superscripts $t = 0$ and $t = 1$ stand for the isoscalar and isovector part of the corresponding densities, as for example,

$$\rho^{(0)}(r) = \rho_n(r) + \rho_p(r), \quad \rho^{(1)}(r) = \rho_n(r) - \rho_p(r). \quad (2)$$

The coefficients C are taken to be constants except for C_t^{ρ}, which depends on the isoscalar density $\rho^{(0)}$ according to the parametrization,

$$C_t^{\rho}(\rho^{(0)}) = C_t^{\rho}(0) + \left(C_t^{\rho}(\rho_{\rm sat}) - C_t^{\rho}(0)\right)\left(\frac{\rho^{(0)}}{\rho_{\rm sat}}\right)^{\alpha}, \quad (3)$$

where $\rho_{\rm sat}$ is the saturation density in infinite symmetric nuclear matter. See Appendix A and Ref. [21] for additional definitions.

This functional depends on the occupied single-particle orbitals in a complex way because of the presence of kinetic densities and currents. A simpler dependence on the single-particle densities ρ_q can be obtained using a semiclassical Wigner-Kirkwood expansion [1], which is the basis of the so-called Thomas-Fermi approximation. We will consider an expansion up to the second $\hbar^2$ order. The kinetic density $\tau^{(0)}$ reads at the zeroth order (Thomas-Fermi approximation) [1]

$$\tau^{(0)} = \tau_{\rm TF} \equiv \frac{3}{5}(3\pi^2)^{(2/3)}\sum_q \rho_q^{5/3}, \quad (4)$$

and at the second order $\tau^{(0)} = \tau_{\rm TF} + \sum_q \tau_{q,2}^{L} + \tau_{q,2}^{NL}$ where,

$$\tau_{q,2}^{L} = \frac{1}{36}\frac{(\nabla\rho_q)^2}{\rho_q} + \frac{1}{3}\Delta\rho_q, \quad (5)$$

$$\tau_{q,2}^{NL} = \frac{1}{6}\frac{\nabla\rho_q\cdot\nabla f_q}{f_q} + \frac{1}{6}\rho_q\frac{\Delta f_q}{f_q} - \frac{1}{12}\rho_q\left(\frac{\nabla f_q}{f_q}\right)^2 + \frac{1}{2}\left(\frac{2m}{\hbar^2}\right)^2\rho_q\left(\frac{W_q}{f_q}\right)^2. \quad (6)$$

Here, $\tau_{q,2}^{L}$ is the second-order local term, $\tau_{q,2}^{NL}$ is the second-order nonlocal term, and the effective mass factor $f_q = m/m_q^*$ is defined as

$$f_q = 1 + \frac{2m}{\hbar^2}\left[\left(C_0^{\tau} + C_1^{\tau}\right)\rho_q + \left(C_0^{\tau} - C_1^{\tau}\right)\rho_{\bar{q}}\right]. \quad (7)$$

.

The spin-orbit current obtained at the same $\hbar^2$ order in the semiclassical expansion is given by [1]

$$J_q = -\frac{2m}{\hbar^2 f_q}\rho_q W_q, \quad (8)$$

where the spin-orbit potential W_q reads

$$W_q = -\left(C_0^{\nabla J} + C_1^{\nabla J}\right)\nabla\rho_q - \left(C_0^{\nabla J} - C_1^{\nabla J}\right)\nabla\rho_{\bar{q}} + \left(C_0^{J} + C_1^{J}\right)J_q + \left(C_0^{J} - C_1^{J}\right)J_{\bar{q}}. \quad (9)$$

In asymmetric systems, the relation between the spin currents J_n and J_p and the gradient of the densities is given by the solution of the 2×2 system of linear equations [22],

$$\left(\frac{\hbar^2}{2m}f_q + \left(C_0^{J} + C_1^{J}\right)\rho_q\right)J_q + \left(C_0^{J} - C_1^{J}\right)\rho_q J_{\bar{q}} = \left(C_0^{\nabla J} + C_1^{\nabla J}\right)\rho_q\nabla\rho_q + \left(C_0^{\nabla J} - C_1^{\nabla J}\right)\rho_q\nabla\rho_{\bar{q}}. \quad (10)$$

The solutions J_n and J_p of this system are injected in Eq. (8) in order to obtain the expression of W_q in terms of the density gradients.

Let us notice however that in several Skyrme interactions such as SIII, SLy4, SGII, ... the terms in $J^{(t)2}$ in the functional (1) are neglected. The spin-orbit potential W_q given in Eq. (9) is therefore simply related to the gradient densities in these functionals, and we have

$$W_q = -\left(C_0^{\nabla J} + C_1^{\nabla J}\right)\nabla\rho_q - \left(C_0^{\nabla J} - C_1^{\nabla J}\right)\nabla\rho_{\bar{q}}. \quad (11)$$

In principle, fourth-order $\hbar^4$ terms can also be added for an improved predictive power, as it has already been done in previous works [1–3].

Hereafter the Skyrme functional with the kinetic energies and currents approximated within the second-order ETF expansion will be noted $\mathcal{E}_{\rm sky}^{\rm ETF}[\rho^{(0)},\rho^{(1)}]$.

B. Symmetric nuclei and generalized Fermi function solution

The great advantage of the semiclassical ETF approximation is that the nonlocal terms in the energy density functional,

see Eqs. (5), (6), and (9), are entirely replaced by local gradients. As a consequence, the energy functional solely depends on the local particle densities. Thus, the energy of any arbitrary nuclear configuration can be calculated if the density profiles ρ_q are given through a parametrized form.

The ground-state configuration should in principle be obtained from the variational calculation, which in the single density case, $\rho = \rho^{(0)}$ and $\rho^{(1)} = 0$, is reduced to single Euler-Lagrange equation,

$$\frac{\partial \mathcal{E}^{\rm ETF}_{\rm sky}}{\partial \rho} - \boldsymbol{\nabla} \cdot \frac{\partial \mathcal{E}^{\rm ETF}_{\rm sky}}{\partial \boldsymbol{\nabla} \rho} + \Delta \frac{\partial \mathcal{E}^{\rm ETF}_{\rm sky}}{\partial \Delta \rho} = \lambda, \tag{12}$$

where λ is a Lagrange multiplier imposing the correct particle number. The generalization of Eq. (12) to the two-density case realized in isospin-asymmetric nuclei is straightforward [1].

Substituting Eq. (1) into the Euler-Lagrange equation, and using the $\hbar^2$ order in the ETF expansion Eqs. (5), (6), (7), (11), leads to

$$\lambda = \frac{dh}{d\rho} + C^{\nabla}(\boldsymbol{\nabla}\rho)^2 + C^{\Delta}\Delta\rho, \tag{13}$$

with

$$\begin{aligned} C^{\nabla}(\rho) &= \frac{\hbar^2}{2m}\frac{1}{36}\left(\frac{1}{\rho^2} + \frac{3\kappa^2}{f^2}\right) + \frac{C_0^{\nabla J} B_J}{2f^2}, \\ C^{\Delta}(\rho) &= \frac{\hbar^2}{2m}\frac{1}{3}\left(-\frac{1}{6\rho} + \frac{7}{3}\kappa - \frac{\kappa}{2f}\right) - 2C_0^{\Delta\rho} + C_0^{\nabla J} B_J \frac{\rho}{f}, \\ h(\rho) &= \frac{\hbar^2}{2m} f \tau_{\rm TF} + \rho^2 C_0^{\rho}, \end{aligned} \tag{14}$$

where the following quantities have been introduced: $\kappa = 2m/\hbar^2 C_0^{\tau}$, $B_J = 2m/\hbar^2 C_0^{\nabla J}$, $f = 1 + \kappa\rho$. This equation was solved, within a simplified energy functional and in the semi-infinite slab geometry, in Ref. [2]. A numerical solution of the Euler-Lagrange equations for finite nuclei employing more general density functionals, including the Coulomb interaction and possibly $\hbar^4$ terms in the semiclassical expansion, is as numerically demanding as the resolution of the HF equations. For this reason, trial density profiles containing only a few variational parameters are often employed [1–3,7–9]. In particular, in Ref. [2] it was shown that a trial density presenting the correct asymptotic behaviors in the one-dimensional system, is given by the generalized Fermi-Dirac distribution (GFD):

$$\rho_{\rm GFD}(r) \equiv \frac{\rho_{\rm sat}}{(1 + \exp(r - R_\nu)/a_\nu)^\nu}. \tag{15}$$

The parameter $\rho_{\rm sat}$ coincides with the solution of the Euler-Lagrange equation in the limit of infinitely extended nuclei, which is the saturation density of symmetric nuclear matter. The other parameters a_ν, R_ν, and ν are analytically derived from the asymptotic solution of the Euler-Lagrange equation [2]. Details are given in Appendix B.

For the nuclear interactions considered in this work, the terms in $J^{(t)2}$ in the functional (1) are neglected. The correction to the Euler equation (13) induced by the inclusion of the spin-orbit current is given in Appendix C.

C. Simple Fermi function model

The variational approach presented in Sec. II B allows an analytical determination of the nuclear energy for symmetric $N = Z$ nuclei. Unfortunately, the generalization of these equations to asymmetric nuclei is highly nontrivial [23] unless severe approximations are assumed. Since our aim is to have a robust model, which can be applied for exotic nuclei as well as for dilute nuclear clusters present in the (proto)neutron star crust, we shall not consider uncontrolled approximations. We shall therefore propose a modified functional form, which is inspired by the solution of the Euler-Lagrange equations, and is directly optimized on Hartree-Fock calculations.

In Ref. [18] an analytical modeling of the density profile was proposed, using a simple $\nu = 1$ Fermi-Dirac (FD) functional form.

$$\rho_{\rm FD}(r) \equiv \frac{\rho_{\rm sat}(\delta)}{1 + \exp(r - R)/a}. \tag{16}$$

Similarly to the previous model given by Eq. (15), the parameter $\rho_{\rm sat}(\delta)$ matches with the limit of infinitely large nuclei, but this time can be generalized in asymmetric matter. The asymmetry dependence of the saturation density is well given by the following form [18],

$$\rho_{\rm sat}(\delta) = \rho_{\rm sat}\left(1 - \frac{3L_{\rm sym}\delta^2}{K_{\rm sat} + K_{\rm sym}\delta^2}\right). \tag{17}$$

In this expression, $L_{\rm sym} = 3\rho_{\rm sat}\partial\mathcal{E}^{\rm sym}_{\rm sky}/\partial\rho^{(0)}$ and $K_{\rm sym} = 9\rho^2_{\rm sat}\partial^2\mathcal{E}^{\rm sym}_{\rm sky}/\partial\rho^{(0)2}$ are the slope and curvature of the symmetry energy at saturation, where we have introduced the usual definition of the symmetry energy functional:

$$\mathcal{E}^{\rm sym}_{\rm sky}(\rho^{(0)}) = \frac{1}{2}\rho^{(0)2}\frac{\partial^2\mathcal{E}^{\rm ETF}_{\rm sky}}{\partial\rho^{(1)2}}\bigg|_{\rho^{(1)}=0}. \tag{18}$$

In Eq. (17), the parameter $\delta = 1 - 2\rho_{{\rm sat},p}/\rho_{\rm sat}$ is the bulk asymmetry of the nucleus. The bulk asymmetry differs from the global asymmetry of the nucleus, $I = 1 - 2Z/A$, because of the presence of a neutron skin and Coulomb effects. The relation between the bulk asymmetry δ and the global asymmetry I is given by [24–26]:

$$\delta = \frac{I + \frac{3a_C}{8Q}\frac{Z^2}{A^{5/3}}}{1 + \frac{9E_{\rm sym}}{4Q}\frac{1}{A^{1/3}}}, \tag{19}$$

where $E_{\rm sym} = \mathcal{E}^{\rm sym}_{\rm sky}[\rho_{\rm sat}]/\rho_{\rm sat}$ is the symmetry energy at saturation, Q is the surface stiffness coefficient extracted from a semi-infinite nuclear matter calculation, and a_C is the Coulomb parameter taken equal to $a_C = 0.69$ MeV. The radius parameter R entering the density profile (16) is given by

$$R = R_{\rm HS}\left[1 - \frac{\pi^2}{3}\left(\frac{a}{R_{\rm HS}}\right)^2\right], \tag{20}$$

where $R_{\rm HS} = [3A/4\pi\rho_{\rm sat}(\delta)]^{1/3}$ is the equivalent homogeneous sphere radius. Equation (20) can be deduced from the general expression given in Appendix B, Eq. (B13). The diffuseness parameter a of the total density profile is assumed to depend quadratically on δ, $a = \alpha + \beta\delta^2$, where α and β were fitted from HF calculations in Ref. [18].

This simple model has the great advantage that its level of predictivity is the same for symmetric and asymmetric nuclei [18]. To describe an isospin asymmetric system, we need two independent density profiles. We will for this purpose use the total isoscalar density ρ and the proton density ρ_p as two FD functions characterized by the corresponding saturation densities $\rho_{\rm sat}$, and $\rho_{{\rm sat},p} = (1-\delta)/2\rho_{\rm sat}$, diffuseness $a(\delta)$, $a_p(\delta)$ (with parameters $\alpha, \alpha_p, \beta, \beta_p$ governing the diffuseness isospin dependence), and radii R, R_p as given by Eq. (20) above.

Moreover, the extension to the physical situation of the inner crust, where nuclei are immersed in a gas of continuum states, is also relatively straightforward [18]. This point will be discussed in Sec. V.

III. COMPARISON TO HARTREE-FOCK CALCULATIONS

Once the parameters of the density profiles are specified, the nuclear ground-state energy is straightforwardly calculated as

$$E_{\rm ETF} = \int d^3r \mathcal{E}^{\rm ETF}_{\rm sky}[\rho^{(0)}, \rho^{(1)}], \tag{21}$$

where the semiclassical ETF nuclear functional $\mathcal{E}^{\rm ETF}_{\rm sky}$ is given in Sec. II A. In this expression, the isoscalar and isovector densities are calculated imposing FD profiles for the total isoscalar and proton densities ρ and ρ_p. For symmetric nuclei the isovector density $\rho^{(1)}$ vanishes and it becomes possible to describe the density profile with a GFD profile via Eq. (15), which in principle should be more correct since it corresponds to the variational solution of the ETF problem, though using a trial density profile.

The quality of the models given by Eqs. (15) and (16) can be judged by comparing the ansatz density profiles and the associated energies to HF calculations performed with the same nuclear effective interaction. For these numerical applications, we will systematically use the SLy4 Skyrme nuclear interaction [17]. We first compare the GFD (15) and FD (16) ansatz density profiles for $N = Z$ nuclei, showing the minor role of the parameter ν as well as the limitations of the variational approach.

A. Comparison between FD and GFD ETF in symmetric nuclei

Figure 1 shows the density profiles, as well as the density multiplied by r^2 and the gradient of the density $\times r^2$ for some chosen representative $N = Z$ nuclei. In all cases, the GFD (16) and FD (15) ansatz density profiles are compared to Hartree-Fock calculation in spherical symmetry. Double magic nuclei are considered in the left part of the figure, while open shells ones are plotted in the right part.

We can see that both the FD and the GFD ansatz can reproduce the HF density profiles with the same accuracy and, quite interestingly, the diffuseness of the nuclear surface is equally well reproduced by the two ansatz. Microscopic density profiles exhibit ripples in the central density, which are not accessible to a simple (G)FD shape. However, these structures are not expected to influence the energetics of the system in an important way, because of the volume element

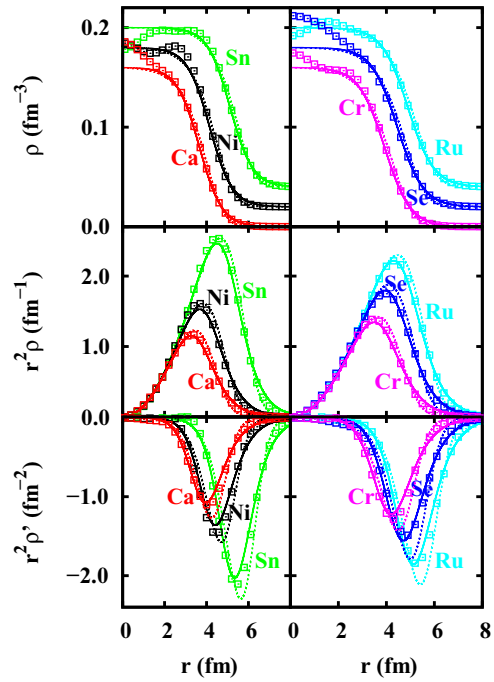

FIG. 1. (Color online) Density profiles (top), corresponding particle numbers (center), and density derivative profile times r^2 (bottom) of different magic (left, ^{40}Ca, ^{56}Ni and ^{100}Sn) and open-shell (right, ^{48}Cr, ^{68}Se, ^{88}Ru) even-even symmetric nuclei. Symbols: spherical HF calculations. Dashed lines: GFD model Eq. (15). Solid lines: FD model Eq. (16). A vertical shift of $\delta\rho = 0.02(0.04)$ fm^{-3} is applied to the density profiles of ^{56}Ni, ^{68}Se (^{100}Sn, ^{88}Ru) to better separate the different curves.

in the energy integral. Moreover, it is known that they are to a large extent artifacts of the mean-field approach and are expected to be washed out by correlations. For these reasons, the densities and the gradient of the densities are multiplied by r^2 in the lower panels of Fig. 1. Interesting enough, the GFD functional form, even multiplied by r^2, does not give a better reproduction of the microscopic calculations than the simpler FD one. It is clear from this figure that the FD profile is flexible enough to reproduce the gross features of the microscopic calculation. In particular we can see that the fall-off of the density in the HF calculation is very well described by an exponential behavior. Conversely, it was shown in Ref. [3] that the variational ETF solution exhibits a slower polynomial decrease when the $\hbar^4$ terms are included. This is again an argument suggesting that we can safely neglect these higher-order terms. It is also important to remark that the Coulomb interaction is known to affect the density profile, though it can be considered as a second order effect. The Coulomb effects are implicitly included in the FD model of Sec. II C, while both the direct and exchange term of the Coulomb energy density should be included in the Euler-Lagrange equations for a correct derivation of the density profile if we use the variational strategy of Sec. II B.

The satisfactory performance of the FD model is confirmed and quantified by Fig. 2, which displays the energy per particle of $N = Z$ nuclei as a function of their mass number. Only the

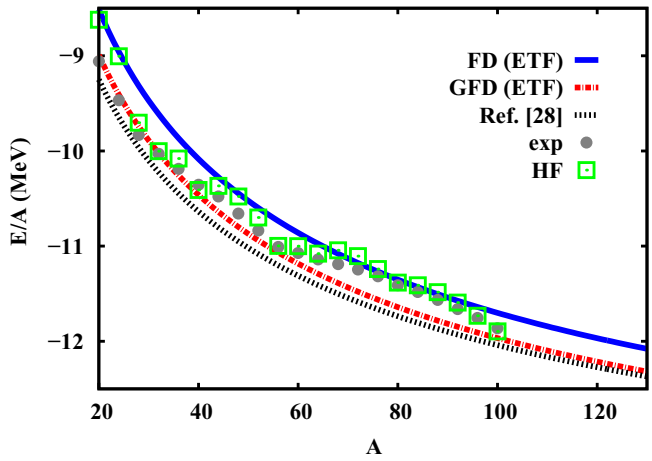

FIG. 2. (Color online) Energy per nucleon of $N = Z$ nuclei as a function of the mass number. Squares: HF calculations; circles: experimental data from Ref. [27]. Solid blue line: FD model. Dashed red line: GFD model. Dotted black line: results from Ref. [28].

nuclear part of the HF energy is considered in this figure. For consistency, the same Coulomb energy, as obtained in HF, is subtracted from the experimental nuclear masses, taken from Ref. [27].

We can see that the GFD profiles systematically produce more binding than the FD ones, as expected from the wider variational space associated to this functional form. The resulting energies are in good agreement with both the microscopically calculated and measured masses for the magic nuclei represented in Fig. 1 above. However, the other nuclei are overbound. This overbinding is known to be due to the absence of fourth-order terms in the ETF functional [3]. The simpler FD model with no variationally determined parameter underbinds magic nuclei, but it leads to an overall good agreement with the microscopic calculations. These results are consistent with previous findings comparing FD and GDF ansatz profiles [3].

A liquid-drop-like parametrization for the nuclear masses in the framework of mean-field Skyrme models was recently proposed in Ref. [28]. In this reference, the authors propose the following functional form for the nuclear energy

$$E_{\rm LDM} = a_v A - a_s A^{2/3} - \frac{a_v^a}{1 + \frac{a_v^a}{a_s^a A^{1/3}}} A I^2, \qquad (22)$$

and have extracted the parameters a_v, a_s, a_v^a, a_s^a from a fit of HF calculations in an uncharged semi-infinite geometry, as well as from the neutron-proton radii differences. The isoscalar part of Eq. (22) contains bulk and surface contributions only while the isovector part contains additionally curvature and beyond contributions. The result of Eq. (22), using the same SLy4 functional [17], is also displayed in Fig. 2. We can see that the variational ETF calculation correctly converges towards the slab estimation (22) for very large mass numbers, where curvature corrections to the surface energies due to the spherical geometry are becoming negligible. The functional form given by Eq. (21) naturally contains curvature effects in the isoscalar and isovector channel. The difference between Eqs. (21) and (22) is mostly due to the missing curvature term in the isoscalar channel in Eq. (22). For light nuclei Eq. (22) therefore tends to overestimate the binding.

From the ensemble of results presented in Fig. 2 we can conclude that the ansatz densities FD and GFD reproduces equally well the microscopic HF calculations, and that the biggest source of discrepancy is mainly due to the lack of shell effects in the ETF approach. We therefore stick to the FD parametrization, and turn to test its predictivity in asymmetric nuclei, where a direct analytical solution of the Euler-Lagrange equations does not exist with any trial density profile.

B. Comparison between HF and FD ETF in asymmetric nuclei

Some representative microscopic HF density profiles are compared to the FD ansatz (16) in Fig. 3. We can see that the level of agreement with the microscopic calculation is comparable to the case of symmetric nuclei. It does not depend on the exoticity of the nucleus but mostly on the size of the system. The larger the system, the better the FD model. This statement is better quantified in Fig. 4, which shows the energy difference between the ETF calculation and the microscopic one as a function of the neutron number, for some selected isotopic chains. In this figure, the filled symbols correspond to the Thomas-Fermi or local density approximation, consisting in truncating the kinetic energy density expansion to the zero order in $\hbar$, see Eq. (4). In this approximation, which was used in a previous work [18], the spin-orbit term vanishes and the local kinetic energy density at a position r is the same as for infinite nuclear matter at the local density $\rho(r)$, $\rho_p(r)$. We can see that the inclusion of second-order terms in the functional (open symbols in Fig. 3) considerably improves the description. In particular, for the heaviest isotopic chain considered, the average ETF energy very well reproduces the average HF energy. The deviations are comparable to the difference between the HF model and the experimental data (solid circles), and can be fully ascribed to the missing shell

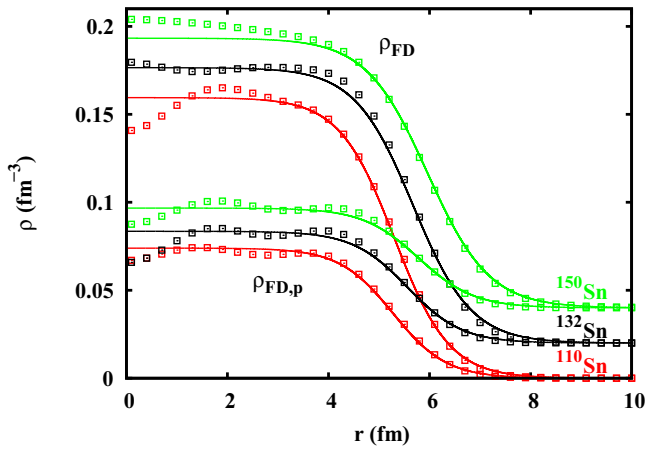

FIG. 3. (Color online) Total (upper curves) and proton (lower curves) density profiles of different Sn isotopes. Symbols: spherical HF calculations. Solid lines: FD model Eq. (16). A vertical shift of $\delta\rho = 0.02(0.04)$ fm^{-3} is applied to the density profiles of ^{132}Sn (^{150}Sn), to better separate the different curves.

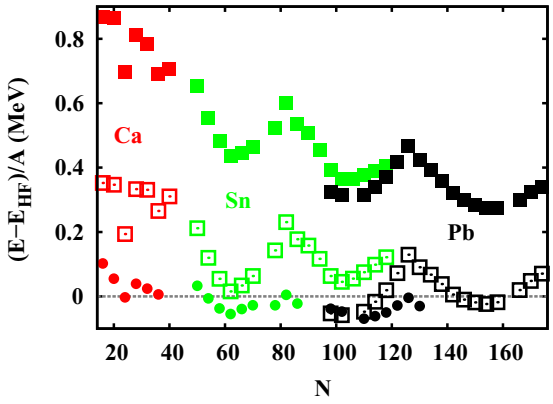

FIG. 4. (Color online) Difference between the energy per particle calculated in the ETF model and in the HF for the isotopic chain of Ca (red symbols), Sn (green symbols), and Pb (black symbols). Solid squares: zeroth-order TF approximation. Open squares: second-order $\hbar$ expansion. Solid circles: experimental data.

effects. These effects, which cannot be accounted for by a semiclassical model as ETF, could in principle be included with Strutinsky smoothing techniques [7]. For the application to the protoneutron star crust that we are interested in, however, we do not expect this to be an important point, as shell effects are known to rapidly wash out with increasing temperature.

To conclude, the use of the simple FD ansatz in the ETF approach at second order in $\hbar$ has been found to reproduce with a good accuracy the microscopic HF density profiles as well as the HF binding energies, with an accuracy of the order of 300 keV/nucleon for the lighter nuclei, and which does not exceed 150 keV/nucleon for the heavy ones. A significant improvement is found with respect to the previous work [18].

IV. SYMMETRY ENERGY FROM ETF

Let us now turn to a first application of the model. Given the reasonably good reproduction of the smooth part of the microscopic nuclear density, the ETF description can be used to explore the functional form of the nuclear mass, and in particular the separation in a bulk and surface term of its isovector and isoscalar parts.

Such a separation is important for the extraction of the largely unknown density behavior of the symmetry energy from nuclear data [29]. Indeed it has been proposed in the literature [30] that the symmetry energy can be strongly constrained from the measurement of nuclear masses. These estimations give the experimental constraints on the symmetry energy, which have at present the smallest uncertainties [31]. The determination of the symmetry energy from nuclear mass implies that the surface and bulk component of the isospin dependence can be unambiguously distinguished. However, very different values are reported in the literature for the surface symmetry energy coefficient [32–35]. In a two-component system, there are two possible definitions of the surface energy, which depend on the definition of the bulk energy in the cluster [20,25,36]: the first one corresponds to identifying the bulk energy of a system of N neutrons and Z protons to the energy of an equivalent piece of nuclear matter $E_S = S_{\gamma_e} \equiv E - eA$, where $A = N + Z$ and e is the energy per nucleon of uniform matter. The second definition $E_S = S_{\gamma_\mu} \equiv E - \mu_n N - \mu_p Z + pV$ corresponds to the grand-canonical thermodynamical Gibbs definition. The first definition is the standard surface energy of the droplet model [37], while the second one gives the quantity to be minimized in the variational calculation conserving proton and neutron number. It was shown that the sign of the surface symmetry energy depends on the choice between these two possibilities [20,25,36]. Moreover it was argued [20] that the case of liquid-drop model (LDM) mass formulas, where the bulk energy is a function of the total mass number A and of the global asymmetry $I = (N - Z)/A$ only, is closer (though not equal) to the Gibbs definition. This can explain why LDM mass formulas systematically obtain negative (though widely varying) surface symmetry energy coefficients [32–35].

If the total energy E is exactly known, the two decompositions are in principle exactly equivalent, meaning that the surface symmetry energy is ill defined. However, the total energy is never exactly known. In the case of empirical mass formulas, it is given by a fit of experimental data. In the case of ETF-based functionals, as in the present study, we are seeking for the best possible approximation to the complete variational HF problem within a given effective interaction. Therefore it is important to determine if there is a decomposition that is best suited to reproduce the Hartree-Fock energy. The variational ETF theory imposes the use of local quantities instead of global ones, and it therefore naturally leads to the use of the local asymmetry parameter δ instead of I. This choice implies that the surface symmetry energy shall be positive as we will show hereafter.

A. Surface symmetry energy

In our model, the neutron and proton density profiles are fully defined by the FD ansatz, which conserves the particle numbers by construction and contains no variational parameters. For this reason we do not need to introduce the Gibbs surface tension [20], and will only refer to the definition of the surface energy as the quantity deduced from the total energy after subtraction of the energy the system would have in the absence of the surface:

$$E_S = E_{\rm ETF} - \frac{\mathcal{E}^{\rm ETF}_{\rm sky}[\rho^{(0)} = \rho_{\rm sat}(\delta), \rho^{(1)} = \rho_{\rm sat}(\delta)\delta]}{\rho_{\rm sat}(\delta)} A. \qquad (23)$$

As we have already observed, because of the presence of the neutron skin, the isospin asymmetry distribution is not uniform in the nuclear system. As a consequence, the bulk asymmetry δ does not coincide with the global asymmetry $I = (N - Z)/A$, see Eq. (19). It is clear that the symmetry energy obtained from Eq. (23) will be different if one replaces the subtracted bulk component evaluated at the bulk asymmetry δ by the one evaluated at the global symmetry I. Most mass formulas, both phenomenological [24,30] and microscopically motivated [32–35], assume, however, that the bulk isospin dependence is given by the the global asymmetry variable $I = (N - Z)/A$. This is for instance the case of the reported

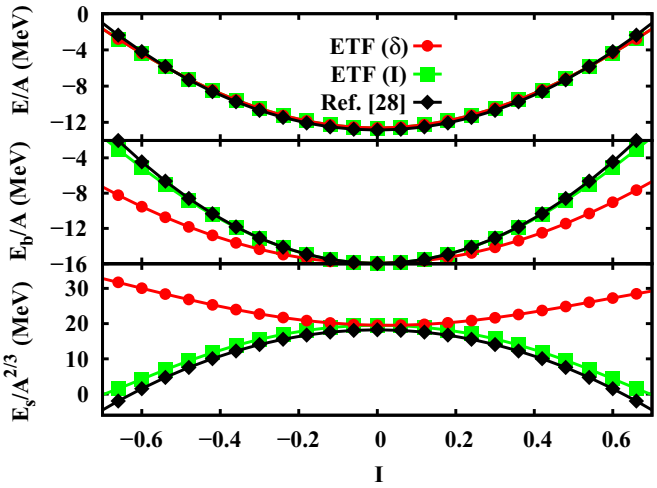

FIG. 5. (Color online) Total (top) and bulk (center) energy per nucleon and surface energy per surface nucleon (bottom) along the isobaric chain $A = 200$. Red circles: ETF calculation including the neutron skin effect Eq. (23) (see text). Green squares: ETF calculation neglecting the neutron skin effect Eq. (25). Black diamonds: estimation from Eq. (24).

Eq. (22) where the surface energy is defined as [28],

$$E_S^{\rm LDM} = E_{\rm LDM} - \left(a_v - a_v^a I^2\right) A. \tag{24}$$

In Fig. 5 are compared, as a function of the global asymmetry I, the energy and the symmetry energy obtained from Eqs. (21) and (23), referred to as ETF(δ), the same energies but replacing δ by I,

$$E'_S = E_{\rm ETF} - \frac{\mathcal{E}^{\rm ETF}_{\rm sky}[\rho_{\rm sat}(I),\rho_{\rm sat}(I)I]}{\rho_{\rm sat}(I)} A, \tag{25}$$

referred to as ETF(I), and the ones obtained from Eqs. (22) and (24), referred to by Ref. [28]. This comparison is performed for a representative isobaric chain $A = 200$. For such heavy nuclei, the curvature terms play a minor role and the liquid-drop formula (24) referred to by Ref. [28] leads to a nuclear energy very close to the ETF model. However, because of the very different partition between bulk and surface in the models EFT(δ) and LDM (24), the surface symmetry energy shows an opposite behavior in the two models. As a consequence, the surface energy, and more specifically the surface symmetry energy, depends on the prescription employed to remove the bulk component, cf. Eqs. (23) and (25).

It is interesting to notice the very close behavior of the surface energies given by ETF(I) and LDM (24) in Fig. 5. This very similar behavior asserts the important role of the asymmetry parameters δ and I. Specifically, the isospin dependence of the symmetry energy shown also in Fig. 5 is found to behave in an opposite way between the models EFT(δ) and the two other models ETF(I) and LDM (24). Consistently with Ref. [20], it can be deduced from the curvature of the curves represented in the bottom panel of Fig. 5 that the choice of the asymmetry variable has an important consequence on the sign of the surface symmetry energy.

This effect is easy to understand analytically. Let us start from the relation between the bulk asymmetry δ and the global asymmetry I previously given by Eq. (19). In the limit of small asymmetries, neglecting the Coulomb correction and fixing $x = 3a_C/8Q$ and $y = 9E_{\rm sym}/4Q$, we can make the approximation

$$\delta^2 = \left(\frac{I + xA^{1/3}(1-I)^2}{1 + yA^{-1/3}}\right)^2 \approx I^2[1 - 2yA^{-1/3} + g(A,I)], \tag{26}$$

where the residual term $g(A,I)$ contains terms of order x, y^2 or smaller, which can be viewed as a correction with respect to the previous term. We can see that the replacement of the asymmetry parameter δ by I in Eq. (26), induces a correction to the LDM, which is proportional to $A^{-1/3}$. This means that the ambiguity in defining the proper asymmetry parameter in the bulk term of the LDM propagates to the surface term. Moreover, replacing δ by I in the LDM induces an extra surface symmetry term with a negative sign, cf. Eq. (26). Since the surface symmetry term is positive in ETF(δ), the change of sign in ETF(I) can be related to the negative extra term in Eq. (26). In order to set this argument straight, let us now be more quantitative.

In the parabolic approximation [18], the bulk part of the ETF energy (21) is quadratic in δ:

$$E_{\rm ETF} \approx (\lambda_{\rm sat} + E_{\rm sym}\delta^2)A + E_S(A,I), \tag{27}$$

where $\lambda_{\rm sat} = \mathcal{E}^{\rm ETF}_{\rm sky}(\rho_{\rm sat},0)/\rho_{\rm sat}$, see Eq. (B4) in the Appendix, and E_S is the surface energy as in Eq. (23), $\lim_{A\to\infty} E_S/A = 0$. If the same parabolic approximation is employed for the bulk term of Eq. (25) as it is customarily done, see Eq. (24),

$$E_{\rm ETF} \approx (\lambda_{\rm sat} + E_{\rm sym}I^2)A + E'_S(A,I). \tag{28}$$

Comparing Eqs. (27) and (28), and using Eq. (26), we immediately get the following relation between the two surface energies,

$$E'_S \approx E_S - \left(\frac{9E_{\rm sym}^2}{2Q}A^{2/3} - Ag(A,I)\right) I^2. \tag{29}$$

It is interesting to remark that this same equation was derived in Ref. [20] as the difference between the microcanonical (γ_e) and grand-canonical (γ_μ) surface energies, in the limit of small asymmetries. This equation shows that the surface energy E'_S contains an extra negative symmetry term due to the nonuniformity of the isospin distribution. As a result, the surface symmetry energy can change from positive to negative, as it is shown in Fig. 5.

B. Curvature symmetry energy

In spherical symmetry it is well known that the surface energy obtained from Eq. (23) does not exactly scale as $A^{2/3}$, but it contains slower varying terms, the dominant one being a curvature term, proportional to $A^{1/3}$. In Fig. 6 is displayed the behavior with the mass number A of the surface energy divided by $A^{2/3}$, where the surface energy is obtained in various ways: the red circles represent the surface energy

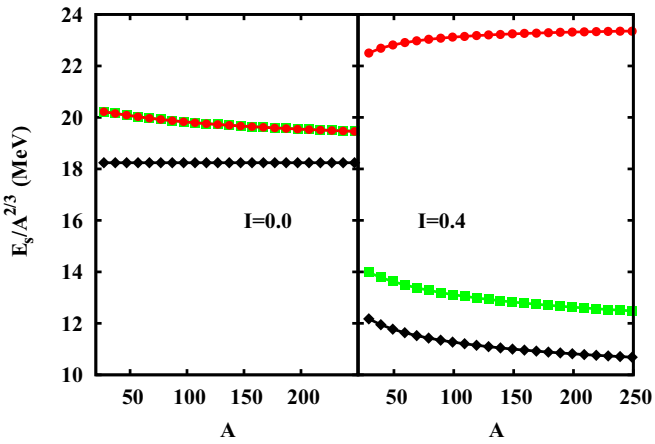

FIG. 6. (Color online) Surface energy per surface nucleon as a function of the nucleus mass. Red circles: ETF calculation including the neutron skin effect Eq. (23) (see text). Green squares: ETF calculation neglecting the neutron skin effect Eq. (25). Black diamonds: estimation from Eq. (24).

defined by Eq. (23), where the bulk asymmetry parameter δ is employed taking into account the nonuniformity of the isospin asymmetry distribution in nuclei due to the presence of a neutron skin; the green squares are obtained from Eq. (25), where the bulk asymmetry is approximated by the global asymmetry parameter I; and the black diamonds stand for surface energy deduced from the LDM (24). The left panel of Fig. 6 shows the isoscalar behavior of the surface energy, where the global asymmetry is fixed to be $I = 0$, while the right panel shows the result by fixing the asymmetry parameter to a finite value $I = 0.4$. Apart from the LDM (24) in the isoscalar case, it is observed that the surface energy is not constant, revealing the presence of a curvature energy in the considered models.

We can see from the left panel of Fig. 6 that the isoscalar curvature energy is positive for the ETF models (23) and (25), and zero for the LDM (24). The absence of the curvature energy in the isoscalar part of the functional (24) is due to the fact that this LDM formula was motivated by one-dimensional slab calculations [28], which by definition do not contain this term. The absence of a curvature energy is at the origin of the poorer reproduction of nuclear masses for symmetric nuclei, as observed in Fig. 2.

For the isoscalar case, there is almost no difference between the asymmetry parameters I and δ, therefore the surface energies (23) and (25) overlap on the left panel of Fig. 6. On the right panel of Fig. 6 where $I = 0.4$ the symmetry energy (23) is shifted up, and the symmetry energies (25) and (24) are shifted down, as expected from Fig. 5. The curvature in the case $I = 0.4$ is, however, given by a mixture of isoscalar and isovector contributions. The effect of the isovector term in the case of the surface energy (23) is, however, sufficiently negative to overcome the isoscalar contribution. We can therefore deduce from Fig. 6 that the curvature energy is positive and the asymmetry curvature energy is negative in the case of Eq. (23). In the case of the model (25), the isovector term goes in the same direction as the isoscalar term, and the trend of the surface symmetry is similar to the one from the LDM (24). We can see from Fig. 6 that again the sign of the surface symmetry term is opposite in the ETF models (23) and (25), and that the ETF model neglecting the neutron skin effect (25) has the same behavior as the mass formula (24).

This is again coming from the bulk contribution subtracted in the two ETF models (23) and (25). Indeed Eq. (29) shows that the difference between bulk δ and global I isospin parameters induces an extra mass-dependent term, which contributes negatively to the curvature surface symmetry energy. Neglecting the nonuniform isospin density distribution, induced by neutron skin and Coulomb repulsion, a positive symmetry curvature energy is obtained, while taking into account the nonuniformity of the isospin density distribution, a negative sign is found.

C. Hints from Hartree-Fock

According to the discussion in Secs. IV A and IV B, an ambiguity exists in the definition and in the sign of the surface symmetry energy, as well as of the curvature symmetry energy. This ambiguity arises from the fact that the bulk asymmetry of nuclei δ differs from their global asymmetry I because of the presence of a neutron skin and, to a minor extent, to the distortion of the density profile due to the Coulomb interaction. Since $I = \delta$ at the thermodynamic bulk limit, *a priori* both Eqs. (23) and (25) can be proposed as a definition of the surface energy, and one may conclude that the surface symmetry energy is ill defined.

At the level of the ETF approximation however, these two equations are not equivalent and only Eq. (23) is theoretically justified. Indeed, as we have discussed in Sec. II B, if we consider only ground-state configurations, the ETF approximation is equivalent to the solution of a set of coupled local Euler-Lagrange equations. In the idealized situation of a system with a locally constant density profile $[\rho_q'(r) = \rho_q''(r) = 0$ for a given value of $r = r_0]$, these equations simply read

$$\lambda_q = \frac{\partial h}{\partial \rho_q}(r_0). \tag{30}$$

This equation admits the simple local bulk solution $\rho_q(r_0) = \rho_{\mathrm{sat},q}$, where the saturation density $\rho_{\mathrm{sat},q}$ has to be calculated at the asymmetry $\delta(r_0) = 1 - 2\rho_p(r_0)/\rho(r_0)$, that is the local asymmetry. This reasoning implies that the bulk energy has to be calculated with the local bulk asymmetry δ.

Another argument going in the same direction comes from a comparison to HF calculations. Indeed, for the quantity defined in Eq. (25) to vanish at the bulk limit, the $\rho_{\mathrm{sat},q}$ parameters entering the proton and neutron density profiles should be identified with $\rho_{\mathrm{sat},q} = (1 \pm I)/2\rho_{\mathrm{sat}}(I)$, and the one entering the total isoscalar density should read $\rho_{\mathrm{sat}} = \rho_{\mathrm{sat}}(I)$. Replacing these quantities in Eq. (16) leads to a different model both for the density profiles and for the ETF energy according to Eq. (21). This alternative model, noted ETF(I) to distinguish it from the ETF(δ) proposed in Sec. II C, can be compared to HF calculations using the same Skyrme functional. This comparison in shown in Table I for the representative case of the total energy per nucleon and proton mean radius along the Pb isotopic chain.

TABLE I. Comparison between HF and ETF along the Pb isotopic chain. The different columns give, from left to right: the mass number of the isotope, the average isospin asymmetry, the bulk isospin asymmetry [Eq. (19)], the mean HF proton radius, the percentage deviation in the mean proton radius between HF and the ETF(I) and the ETF(δ) models, the HF energy per nucleon, and the percentage deviation in the energy per nucleon between HF and the ETF(I) and the ETF(δ) model. The last line gives the arithmetic average along the isotopic chain.

A	I	δ	$\bar{r}_p(HF)$	$\%(I)$	$\%(\delta)$	E_{HF}/A	$\%(I)$	$\%(\delta)$
180	0.09	0.08	5.31	−0.5	−1.1	−12.25	−0.3	−0.4
196	0.16	0.13	5.40	+0.8	−0.5	−11.93	+0.4	−0.1
216	0.24	0.19	5.50	+2.7	+0.4	−11.34	+1.8	+0.5
236	0.31	0.25	5.67	+3.4	+0.0	−10.51	+1.8	−0.2
256	0.36	0.29	5.77	+5.0	+0.6	−9.81	+3.6	+0.7
⟨⟩	0.23	0.19	5.53	+2.3	−0.1	−11.17	+1.4	+0.1

We can see that the ETF(δ) model systematically gives a better reproduction of HF results, and the deviation between ETF(δ) and ETF(I) increases with increasing difference between bulk δ and global I asymmetry parameters. The HF result supports the intuitive idea behind Eq. (16), which is related to the local character of the Euler-Lagrange variational equations: the density in the bulk of a heavy nucleus is related to the saturation density corresponding to the local bulk asymmetry, and not to the global asymmetry of the nucleus.

In conclusion, these two arguments show that the model EFT(δ) is better justified both from a theoretical point of view and from a comparison to HF calculations. The bulk energy shall therefore be parameterized in terms of the bulk asymmetry, and the surface symmetry energy in the corresponding LDM shall be positive.

V. NUCLEI IMMERSED IN A NUCLEON GAS

We now turn to the second application of this model, which concerns the evaluation of the in-medium modification of the nuclear ground-state energy due to the presence of a surrounding nuclear gas of unbound nucleons. Having in mind the evaluation of the equation of state and structure of supernova matter [19], we have to consider excited states of arbitrarily high energy. Above the particle separation threshold, vibrations and deformations can be neglected and the excited configurations essentially correspond to the coexistence of nuclei of arbitrary isospin with a uniform neutron gas composed both of protons and neutrons. The extension of the formalism presented in Sec. II C to this situation was already presented in Ref. [18]. Here we give only the main points of the model, and address the reader to Ref. [18] for further details. In a Wigner-Seitz cell occupied by a uniform nucleon gas with densities $\rho_{g,q}$, the total density profile of protons and neutrons in the cell can be decomposed into a cluster and a gas component. Due to the high nuclear incompressibility, we assume that the bulk density of the clusters is not modified by the occupation of unbound particle states [18]. Equation (16) is then replaced by a more general ansatz, including the uniform gas, and given by

$$\rho_{\mathrm{FD},q}(r) \equiv \frac{\rho_{\mathrm{sat},q}(\delta) - \rho_{g,q}}{1 + \exp(r - R_q)/a_q} + \rho_{g,q}. \tag{31}$$

The bulk asymmetry δ of the cluster has also to be modified from the vacuum expression Eq. (19) in order to include the overlap of the cluster with the uniform gas. Indeed Eq. (19), being an equation for a bound nucleus, applies only to the bound part of the cluster A_e. In the spirit of the independent particle model, this bound part can be defined as the ensemble of bound states, obtained from the total number of particles with the subtraction of the gas contribution,

$$A_e = [1 - \rho_g/\rho_{\mathrm{sat}}(\delta)]A; \quad Z_e = [1 - \rho_{g,p}/\rho_{\mathrm{sat},p}(\delta)]Z, \tag{32}$$

where $\rho_g = \rho_{g,n} + \rho_{g,p}$ is the total isoscalar gas density.

The bulk asymmetry δ_e of the ensemble of bound cluster states is given by Eq. (19) with $A = A_e$, $Z = Z_e$ and $I = 1 - 2Z_e/A_e$, while the local asymmetry in the bulk of the cluster is estimated as a linear combination of the asymmetries coming from the bound and the unbound components:

$$\delta = \left(1 - \frac{\rho_g}{\rho_{\mathrm{sat}}(\delta)}\right)\delta_e + \frac{\rho_g}{\rho_{\mathrm{sat}}(\delta)}\delta_g, \tag{33}$$

where $\delta_g = 1 - 2\rho_{g,p}/\rho_g$ is the gas asymmetry.

The total energy in the presence of a gas is still given by Eq. (21), but it now depends both on the cluster and on the gas density profiles through Eq. (31):

$$E^{\mathrm{tot}}_{\mathrm{ETF}} = \int \mathcal{E}^{\mathrm{ETF}}_{\mathrm{sky}}[\rho_{\mathrm{FD},n} + \rho_{\mathrm{FD},p}, \rho_{\mathrm{FD},n} - \rho_{\mathrm{FD},p}]d^3r$$
$$= E^{\mathrm{tot}}_{\mathrm{ETF}}(A, \delta, \rho_g, \delta_g). \tag{34}$$

For an application to the equation of state at finite temperature for supernovae matter [12–15], all the possible values of A, δ, ρ_g, and δ_g have to be considered, and the relative weight of the different configurations is given by the Boltzmann factor. If we limit ourselves to a neutron-rich nuclear cluster embedded in a pure neutron gas, the quality of the model can again be judged in comparison to HF calculations. In Ref. [18], it was shown that the quality of reproduction of complete HF results of this model is almost independent of the presence of an external gas.

The presence of a nucleon gas obviously modifies the energy of the nuclear cluster. The in-medium modification of the cluster energy δE_m can be computed by subtracting to the total energy the contribution of the gas alone and of the nucleus alone, according to [18,19]:

$$\delta E_m = E^{\mathrm{tot}}_{\mathrm{ETF}} - E_{\mathrm{ETF}}(A, Z) - V_{\mathrm{WS}}\mathcal{E}^{\mathrm{ETF}}_{\mathrm{sky}}[\rho_g, \rho_g\delta_g], \tag{35}$$

where V_{WS} is the total volume of the Wigner-Seitz cell, and $E_{\mathrm{ETF}}(A, Z)$ is the energy of a nucleus (A, Z) in the vacuum defined by Eq. (21). We can also express $E_{\mathrm{ETF}}(A, Z)$ from Eq. (23) as

$$E_{\mathrm{ETF}}(A, Z) = \frac{\mathcal{E}^{\mathrm{ETF}}_{\mathrm{sky}}[\rho_{\mathrm{sat}}(\delta), \rho_{\mathrm{sat}}(\delta)\delta]}{\rho_{\mathrm{sat}}(\delta)}A + E_S. \tag{36}$$

Finally the total ETF energy can be decomposed as

$$E^{\rm tot}_{\rm ETF} = \int_0^{R_{\rm HS}} \mathcal{E}^{\rm ETF}_{\rm sky}[\rho^{(0)},\rho^{(1)}]d^3r + \int_{R_{\rm HS}}^{R_{\rm WS}} \mathcal{E}^{\rm ETF}_{\rm sky}[\rho^{(0)},\rho^{(1)}]d^3r$$
$$= \mathcal{E}^{\rm ETF}_{\rm sky}[\rho_{\rm sat},\rho_{\rm sat}\delta_{\rm sat}]V_{\rm HS} + \mathcal{E}^{\rm ETF}_{\rm sky}[\rho_g,\rho_g\delta_g] \times (V_{\rm WS} - V_{\rm HS}) + E_{S,m}. \quad (37)$$

and, as shown in Refs. [18,19], the total ETF energy is constituted of both a bulk and a surface term. In Eq. (37), $V_{\rm HS} = A/\rho_{\rm sat}$ the hard-sphere volume of the cluster, and $E_{S,m}$ represents a surface term since the bulk parts have been highlighted.

Using Eqs. (35)–(37), we can express the total in-medium modification $\delta E_m = \delta E_B + \delta E_S$ as a bulk and a surface term, with

$$\delta E_B = -A\frac{\mathcal{E}^{\rm ETF}_{\rm sky}[\rho_g,\rho_g\delta_g]}{\rho_{\rm sat}(\delta)}; \quad \delta E_S = E_{S,m} - E_S. \quad (38)$$

Since δE_S is proportional to two surface terms deduced from Eqs. (36) and (37), we can expect the following relation to hold: $\delta E_S = c_s A^{2/3}$, where the parameter c_s should have a weak dependence on A, revealing the small effect of the curvature terms. The validity of this decomposition will be explicitly tested below.

Finally the in-medium modified cluster energy, including both the bulk and the surface energy shift, is given by:

$$E_m(A,Z) = E_{\rm ETF}(A,Z) + \delta E_m = E_{B,m} + E_{S,m}, \quad (39)$$

where

$$E_{B,m} = \left(\mathcal{E}^{\rm ETF}_{\rm sky}[\rho_{\rm sat}(\delta),\rho_{\rm sat}(\delta)\delta] - \mathcal{E}^{\rm ETF}_{\rm sky}[\rho_g,\rho_g\delta_g]\right)\frac{A}{\rho_{\rm sat}(\delta)} \quad (40)$$

and

$$E_{S,m} = E_S + \delta E_S. \quad (41)$$

In the next section, the medium modification of the bulk and surface energies are studied. In practice, a large set of calculations is performed, varying the cluster size and isospin asymmetry over a large domain of N and Z covering the whole periodic table well beyond the neutron drip line. Preliminary results with a simpler TF functional (zero order in $\hbar$) were already presented in Refs. [18,19]. As we show in the next sections, the inclusion of higher-order terms slightly modifies the absolute values of the energy shifts, but does not modify the general trends reported in Refs. [18,19].

A. Medium modifications of the bulk energy

The in-medium bulk energy per nucleon $E_{B,m}/A$, defined by Eq. (40), and computed with the SLy4 interaction is displayed in Fig. 7 as a function of the gas density (left side) for different bulk asymmetries of the nucleus, and as a function of the bulk asymmetry (right side) for different gas densities. Two representative cases are considered: a gas asymmetry equal to the cluster one $\delta_g = \delta$ (bottom panels) and a pure neutron gas $\delta_g = 1$ (top panels).

For very neutron-rich clusters with $\delta \approx 1$, the case $\delta_g = 1$ is relevant both for the ground state of the neutron star inner crust, and for the most representative configurations of neutron-rich matter at finite temperature. For nuclei close to isospin symmetry, $\delta \approx 0$, the case $\delta_g = \delta$ corresponds to the most probable configurations at finite temperature. In all cases, increasing gas density corresponds to physical situations at higher density and/or temperature.

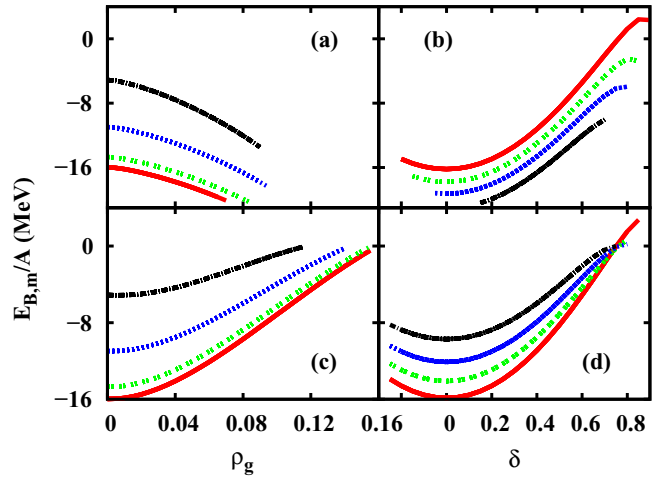

FIG. 7. (Color online) In-medium bulk energy $E_{B,m}/A$, defined by Eq. (40), as a function of the gas density for a fixed bulk asymmetry (left side) and as a function of the bulk asymmetry for a fixed gas density (right side). Top: pure neutron gas ($\delta_g = 1$). Bottom: gas asymmetry equal to the bulk asymmetry ($\delta_g = \delta$). (a) and (c): $\delta = 0.0$ (solid red), $\delta = 0.2$ (dashed green), $\delta = 0.4$ (dotted blue), $\delta = 0.6$ (dash-dotted black). (b) and (d): $\rho_g = 0.01$ (solid red), $\rho_g = 0.04$ (dashed green), $\rho_g = 0.06$ (dotted blue), $\rho_g = 0.08$ (dash-dotted black).

Imposing the gas asymmetry to be strictly equal to the cluster asymmetry, amounts to disregarding isospin effects (isospin fractionation) in the equilibrium. In this case we recover the well known result that the cluster energy is reduced by the presence of the surrounding medium, leading to the dissolution of clusters at the critical Mott density [38,39]. The critical Mott density can be defined as the density corresponding to vanishing bulk binding, and is given by the ending point of each curve in Fig. 7(c). This is the saturation density $\rho_{\rm sat}(\delta)$ and we recover that it monotonically decreases with increasing cluster asymmetry [18].

In the case of stellar matter at β equilibrium the fractionation effect cannot be neglected, and the gas is systematically more neutron rich than the clusters. In particular, in the specific case of cold neutron star crust, the uniform gas is uniquely constituted of neutrons [40]. The limiting case $\delta_g = 1$ is thus close to the physical condition of the low-temperature stellar environment. In this case the trend with respect to the density (at fixed asymmetry δ) is reversed.

The reduction of the in-medium bulk energy with respect to the density at fixed δ is simple to understand: the first term in Eq. (40) is constant at fixed δ, as well as the common factor $A/\rho_{\rm sat}(\delta)$, while the second term in Eq. (40) is increasing with the gas density at fixed $\delta_g = 1$. While this effect seems a bit academic in Fig. 7(a), the consequence of the shift is more interesting to comment in Fig. 7(b). It is

known that in the sequence of nuclei predicted in the crust of neutron stars [40], as the density increases, the asymmetry in the bulk of the nuclear clusters δ also increases. This sequence can be understood in part from Fig. 7(b) since as ρ_g increases, the constant bulk energy path is going towards more and more asymmetric clusters. Taking the sequence of ground-state nuclei predicted in the crust of neutron stars [40], the bulk energy departs from a quadratic behavior with respect of the bulk asymmetry δ [18] since increasing the gas density shifts down the bulk energy, as shown in Figs. 7(a) and 7(b). This simple mechanism explains why clusters can survive in environment extremely neutron rich as neutron star crusts.

It is however surprising that for the gas densities considered in Fig. 7, the medium modifications to the bulk energy remain mostly quadratic with respect to δ at fixed ρ_g. Nonquadraticities in δ are only observed for $\delta \geqslant 0.6$, with or without gas. (right part of Fig. 7). The quadratic dependence of the bulk energy with respect to δ is therefore a robust prediction, which goes beyond the case of isolated nuclei and can be generalized to dilute nuclei to a large extent.

B. Medium modification of the surface energy

Figure 8 illustrates the surface tension, defined as the scaled in-medium surface energy $E_{S,m}/A^{2/3}$, cf. Eq. (41), as a function of the gas density ρ_g and of the bulk asymmetry δ for the same gas compositions as for Fig. 7. The almost perfect scaling with $A^{2/3}$ shows that indeed the in-medium modification of the binding energy is mainly a surface effect. There are only few cases where the curves acquire a finite width, reflecting a small contributions from curvature terms: In Fig. 8(a) where $\delta_g = 1$ and for the most neutron-rich clusters

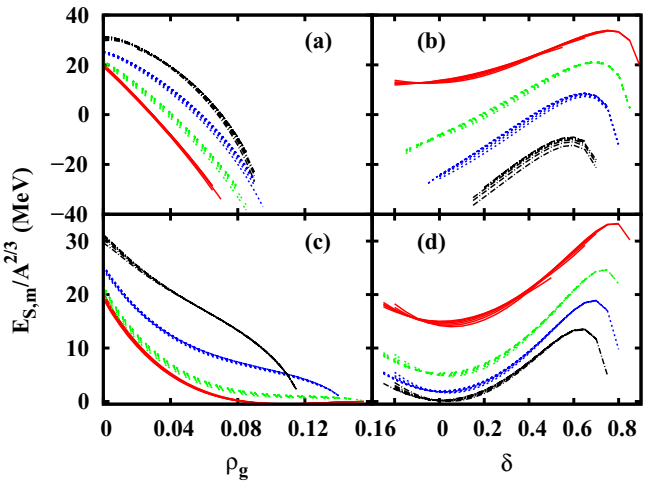

FIG. 8. (Color online) In-medium surface energy [see Eq. (41)] as a function of the gas density for a fixed bulk asymmetry (left) and as a function of the bulk asymmetry for a fixed gas density (right) (see text). Top panels: pure neutron gas. Bottom panels: gas asymmetry equal to the bulk asymmetry. (a) and (c): $\delta = 0.0$ (solid red), $\delta = 0.2$ (dashed green), $\delta = 0.4$ (dotted blue), $\delta = 0.6$ (dash-dotted black). (b) and (d): $\rho_g = 0.01$ (solid red), $\rho_g = 0.04$ (dashed green), $\rho_g = 0.06$ (dotted blue), $\rho_g = 0.08$ (dashed-dotted black).

(black curves), and in Fig. 8(c) where $\delta_g = \delta$ and here also for the most neutron-rich curves (for, e.g., black curves at $\rho_g = 0$). The curvature terms have been discussed in Sec. IV B, and are observed here to be maximal in the most asymmetric clusters as the gas density increases.

Neglecting fractionation effects in Fig. 8(c), the surface energy is reduced as the gas density increases and whatever the cluster asymmetry. It vanishes at the corresponding saturation density $\rho_{\rm sat}(\delta)$, showing again the dissolution of clusters in the dense medium. In Fig. 8(d), the dependence of the surface energy with δ is mostly quadratic, even for the largest densities considered here. The quadratic behavior of the surface energy is well satisfied up to $\delta \geqslant 0.6$, as in the case of the bulk energy.

It is quite surprising to find in the case of pure neutron gas, Figs. 8(a) and 8(b), that the surface energy not only decreases as the gas density increases, but can even become negative. This can be understood from the fact that the surface energy as defined by Eq. (37) represents the interface contribution between the cluster and the gas. At finite gas density, this interface energy contains contributions from both the cluster and the gas. The contribution of the pure neutron gas to the interface region is largely negative, since the interface region is more symmetric than the gas. The negative contribution of the gas dominates as the gas density increases, leading to negative surface energy as shown in Fig. 8(a). This effect is lowered when the cluster is more neutron rich, see Fig. 8(b).

It should also be remarked that the density as which the surface energy becomes negative increases as the bulk asymmetry increases. Since the ground-state configurations predicted for the crust of neutron stars [40], have increasing δ for increasing ρ_g, these configurations always correspond to systems where the surface energy is positive [18,19]. Concerning the dependence of the surface energy on δ in Fig. 8(b), we can see a very different behavior compared with the previous cases: the quadratic approximation in δ is completely lost due to the contribution of the gas, which is not quadratic in δ, but in δ_g.

C. Dependence on the effective interaction

In this section, we show that the qualitative behaviors that we have discussed in this paper are not modified if a different Skyrme interaction is employed. In particular, the positive sign of the surface symmetry energy that we have discussed in Sec. IV A does not depend on the particular effective interaction. However the quantitative values of the clusters bulk and surface energies obviously depend on the effective interaction parameters, and for a realistic treatment of the stellar matter equation of state it is very important to consistently treat within the same effective interaction both the cluster and the free gas [18,19].

To study how the in-medium effects depend on the model, we represent in Fig. 9 two representative situations of a symmetric nucleus in a symmetric gas, and a neutron rich nucleus in a pure neutron gas, with different Skyrme models. We have chosen these specific interactions in order to span the present uncertainties in the bulk parameters. These latter are reported in Table II.

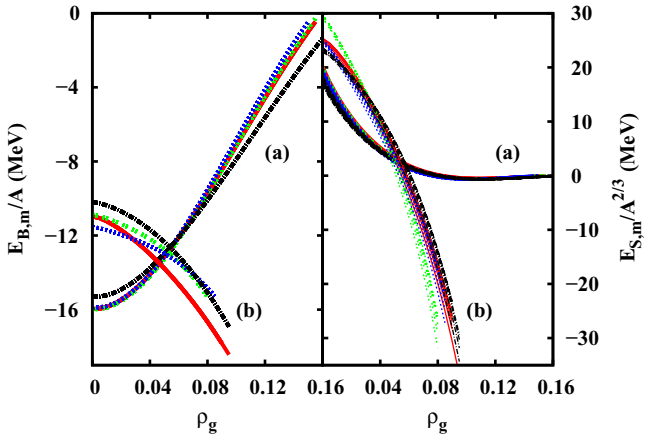

FIG. 9. (Color online) In-medium bulk (left) and surface (right) energy as a function of the gas density (see text). (a): clusters with bulk asymmetry $\delta = 0$ immersed in a symmetric gas. (b): clusters with $\delta = 0.3$ immersed in a pure neutron gas. Different models are considered: Sly4 [17] (solid red), SkI3 [41] (dashed green), SGI [42] (dotted blue), LNS [43] (dash-dotted black).

We can see that the qualitative behavior of the different models is the same. A more complete study of the effective interactions parameter space is needed to reach sound conclusions on the quantitative model dependence, but from the representative chosen interactions we can dress some tentative partial interpretation. The differences in bulk energy directly reflect the uncertainties in present models of the bulk properties of matter. These uncertainties are very small in the isoscalar part, and the curves of the bulk symmetric systems, see curves labeled (a) on the left panel, are indistinguishable except LNS (dashed-dotted black lines). The LNS Skyrme model is known to have a saturation density larger than the expected one, see Table II, which is reflected in the fact that at $\rho_g = 0$ fm^{-3}, the LNS bulk energy is different from the others. It also leads to slightly reduced in-medium modification, as observed in Fig. 9. Concerning medium modifications to the bulk energy in the neutron rich system, see curves labeled (b) on the left panel, it is observed that SLy4 Skyrme interaction (solid red) leads to slightly more important binding energy shift. This is due to a nontrivial interplay of slightly different values of $E_{\rm sym}$, $L_{\rm sym}$, $K_{\rm sym}$. Concerning the surface energies, the behavior appears very stable. The only exception is the gas density behavior of the neutron-rich system, curves (b) in the right panel, calculated with SkI3 (dashed green). This steep in medium modification is probably due to the very stiff isovector properties of this effective interaction.

TABLE II. Bulk nuclear properties for the different Skyrme interactions examined in this paper.

NN potential	$\rho_{\rm sat}$ (fm^{-3})	K (MeV)	$L_{\rm sym}$ (MeV)	$K_{\rm sym}$ (MeV)	$E_{\rm sym}$ (MeV)
SLY4	0.159	230.0	46.0	−119.8	32.00
SGI	0.154	261.8	63.9	−52.0	28.33
SkI3	0.158	258.2	100.5	73.0	34.83
LNS	0.175	210.8	61.5	−127.4	33.43

To conclude, we can see that, independent of the model, the in-medium modifications are not negligible and should be accounted for in a realistic equation of state. Due to the simple expression (37), these corrections can be tabulated as a function of $(A, I, \rho_{g,n}, \rho_{g,p})$ and straightforwardly introduced in the equation-of-state calculations [18,19] as a modification of the cluster energy functional with no extra computational cost.

VI. CONCLUSIONS

In this paper we have considered a simple analytical modeling of the nuclear density profiles allowing us to calculate nuclear binding energies within the extended Thomas-Fermi approximation at the second order in $\hbar$. Through a comparison to HF calculations for some representative nuclei, we have shown that a simple Fermi-Dirac profile is sufficiently flexible to reach a precision in the energy of the order of a 100–200 keV/nucleon, and the widening of the variational space considering FGD trial densities does not introduce any sizable improvement of the predictive power of the model.

Two different applications of the model were presented. The first one concerns the definition of the bulk and surface part of the symmetry energy of finite nuclei, which is important for the extraction of equation-of-state parameters for astrophysical applications. We have shown that the variational character of the ETF formalism suggests that the bulk part of the nuclear energy depends on the central bulk asymmetry δ rather than on the global asymmetry of the nucleus I, which is usually considered in LDM. This statement, which is confirmed by a detailed comparison to HF calculations, implies that the surface symmetry energy contributes positively to the total symmetry energy of the nucleus. The choice of the global asymmetry parameter I considered in LDM, while not consistent with ETF, explains the ambiguities reported in the literature concerning the sign of the surface symmetry energy.

The second application concerns the evaluation of the in-medium energy shift, which is experienced by a nucleus immersed in the gas of its continuum states, as it is the case in supernova matter and in the inner crust of (proto)neutron stars. We have shown that the presence of an external gas induces both a bulk and a surface energy shift, which depend, in a highly complex and nonlinear way, on the asymmetry of the cluster and the asymmetry and density of the gas. The absolute values of these energy shifts can be comparable to or higher than the nuclear binding energy, meaning that the coexistence of nuclei and free particles in stellar matter cannot be modelized as a mixture of noninteracting nuclear species as it is done in the current models of stellar equations of state [12,14,19].

ACKNOWLEDGMENT

This work has been partially funded by the SN2NS project ANR-10-BLAN-0503 and it has been supported by New-Compstar, COST Action MP1304.

APPENDIX A: COEFFICIENTS OF THE SKYRME FUNCTIONAL

Here we write the coefficients of the Skyrme functional as given by Ref. [21],

$$C_0^\rho = \tfrac{3}{8}t_0 + \tfrac{3}{48}t_3\rho^{(0)\alpha}(r) \quad \text{(A1)}$$

$$C_1^\rho = -\tfrac{1}{8}t_0(2x_0+1) - \tfrac{1}{48}t_3(2x_3+1)\rho^{(0)\alpha}(r) \quad \text{(A2)}$$

$$C_0^{\Delta\rho} = \tfrac{1}{64}[-9t_1 + t_2(4x_2+5)] \quad \text{(A3)}$$

$$C_1^{\Delta\rho} = \tfrac{1}{64}[3t_1(2x_1+1) + t_2(2x_2+1)] \quad \text{(A4)}$$

$$C_0^\tau = \tfrac{1}{16}[3t_1 + t_2(4x_2+5)] \quad \text{(A5)}$$

$$C_1^\tau = \tfrac{1}{16}[-t_1(2x_1+1) + t_2(2x_2+1)] \quad \text{(A6)}$$

$$C_0^{\nabla J} = -\tfrac{3}{4}W_0 \quad \text{(A7)}$$

$$C_1^{\nabla J} = -\tfrac{1}{4}W_0 \quad \text{(A8)}$$

$$C_0^J = -\tfrac{1}{16}[t_1(2x_1-1) + t_2(2x_2+1)] \quad \text{(A9)}$$

$$C_1^J = -\tfrac{1}{16}[-t_1 + t_2]. \quad \text{(A10)}$$

APPENDIX B: ANALYTICAL DENSITY PROFILE FOR SYMMETRIC NUCLEI IN SPHERICAL SYMMETRY

Following the derivation of Ref. [2]. our starting point is the one-dimensional Euler equation given by Eq. (13),

$$\lambda = \frac{dh}{d\rho} + C^\nabla(\nabla\rho)^2 + C^\Delta\Delta\rho. \quad \text{(B1)}$$

In the limit of very large r, this equation simplifies to:

$$\lambda = \frac{1}{36}\frac{\hbar^2}{2m}\left[\left(\frac{\rho'}{\rho}\right)^2 - 2\frac{\rho''}{\rho}\right], \quad \text{(B2)}$$

which gives

$$\rho(r) \propto \mathrm{e}^{-r/a_{\rm out}} \quad \text{with} \quad a_{\rm out} = \sqrt{-\frac{\hbar^2}{2m}\frac{1}{36\lambda}}. \quad \text{(B3)}$$

The value of λ is obtained by considering the bulk limit of Eq. (B1). In this limit we have:

$$\lambda = \left.\frac{\partial\mathcal{E}_{\rm sky}^{\rm ETF}}{\partial\rho}\right|_{\rho_{\rm sat}} = \left.\frac{\mathcal{E}_{\rm sky}^{\rm ETF}}{\rho}\right|_{\rho_{\rm sat}} \equiv \lambda_{\rm sat}, \quad \text{(B4)}$$

where we can recognize $\lambda_{\rm sat}$ as the chemical potential of symmetric nuclear matter at saturation.

Close to the bulk limit, that is for $r \to 0$ and $R_\nu \to \infty$, linearizing Eq. (B1) introducing $\rho(r) = \rho_{\rm sat} + \delta\rho$ gives

$$\lambda_{\rm sat} = \frac{dh}{d\rho}(\rho_{\rm sat}) + \frac{d^2h}{d\rho^2}(\rho_{\rm sat})\delta\rho + C^\Delta(\rho_{\rm sat})\delta\rho'', \quad \text{(B5)}$$

where we have defined $f_{\rm sat} = f(\rho_{\rm sat}) = 1 + \kappa\rho_{\rm sat}$. Solving Eq. (B5) leads to

$$\delta\rho(r) \propto \mathrm{e}^{(r-R_\nu)/a_{\rm in}} \quad \text{(B6)}$$

with

$$\frac{K_{\rm sat}}{9}a_{\rm in}^2 = \frac{\hbar^2}{2m}\frac{1}{3}\left[\frac{1}{6} - \frac{7}{3}\kappa\rho_{\rm sat} + \frac{\kappa\rho_{\rm sat}}{2f_{\rm sat}}\right] - C_0^{\nabla J}B_J\frac{\rho_{\rm sat}^2}{f_{\rm sat}} + 2C_0^{\Delta\rho}\rho_{\rm sat}, \quad \text{(B7)}$$

where $K_{\rm sat} = 9\rho_{\rm sat}\partial^2\mathcal{E}_{\rm sky}^{\rm ETF}/\partial\rho^2|_{\rho=\rho_{\rm sat}}$ is the nuclear matter incompressibility. To achieve the two asymptotic behaviors, the density profile can be represented as a generalized Fermi function (GFD) $\rho = \rho_{\rm GFD} = \rho_{\rm sat}F_\nu$ with

$$F_\nu(r) = (1 + \mathrm{e}^{(r-R_\nu)/a_\nu})^{-\nu}. \quad \text{(B8)}$$

Comparing equations (B3) and (B6) with (B8), we have

$$a_\nu = a_{\rm in}; \quad \nu = \frac{a_{\rm in}}{a_{\rm out}} = \frac{6a_\nu}{\hbar}\sqrt{-2m\lambda_{\rm sat}}. \quad \text{(B9)}$$

The link between the parameter R_ν and the particle number is deduced from the leptodermous series development of a_ν/R_ν of the integral giving the particle number:

$$A = 4\pi\int_0^\infty dr\rho_{\rm GFD}(r)r^2. \quad \text{(B10)}$$

The moments I_ν^m of the GFD ansatz have been calculated in Ref. [44], as,

$$I_\nu^m = \int_0^{+\infty} dr\,F_\nu(r)r^m \simeq \frac{R_\nu^{m+1}}{m+1}\left[1 + (m+1)\sum_{n=0}^{m}\binom{m}{n}\eta_\nu^{(n)}\left(\frac{a_\nu}{R_\nu}\right)^{n+1}\right], \quad \text{(B11)}$$

where

$$\eta_\nu^{(n)} = (-1)^n\int_0^\infty du\left[\frac{1 + (-1)^n\,\mathrm{e}^{-\nu u}}{(1+\mathrm{e}^{-u})^\nu} - 1\right]u^n, \quad \text{(B12)}$$

Replacing in Eq. (B10) gives

$$A = \frac{4}{3}\pi\rho_{\rm sat}R_\nu^3\left[1 + 3\eta_\nu^{(0)}\frac{a_\nu}{R_\nu} + 6\eta_\nu^{(1)}\left(\frac{a_\nu}{R_\nu}\right)^2 + 3\eta_\nu^{(2)}\left(\frac{a_\nu}{R_\nu}\right)^3\right].$$

If $a_\nu \ll R_\nu$ this expression can be inverted giving at third order in the leptodermous expansion:

$$\frac{R_\nu}{R_{\rm HS}} \simeq 1 - \eta_\nu^{(0)}\frac{a}{R_{\rm HS}} + \left[\left(\eta_\nu^{(0)}\right)^2 - 2\eta_\nu^{(1)}\right]\left(\frac{a}{R_{\rm HS}}\right)^2 - \left[\frac{2}{3}\left(\eta_\nu^{(0)}\right)^3 - 2\eta_\nu^{(0)}\eta_\nu^{(1)} + \eta_\nu^{(2)}\right]\left(\frac{a}{R_{\rm HS}}\right)^3, \quad \text{(B13)}$$

where $R_{\rm HS} = (3A/4\pi\rho_{\rm sat})^{1/3}$ is the equivalent homogeneous sphere radius.

In conclusion, the parameters of the GFD ansatz given by the parametric form (15) and (B6) can be determined in the following way: $\rho_{\rm sat}$ is the saturation density of nuclear matter, a_ν is given by Eq. (B8), ν is given by Eq. (B9) and R_ν is given by Eq. (B13).

APPENDIX C: INCLUSION OF THE SPIN-ORBIT CURRENT FOR SYMMETRIC NUCLEI IN SPHERICAL SYMMETRY

The nuclear interactions considered in this work neglect the contribution of the spin-orbit current $J^{(t)2}$ in the functional (1). In this section, we give the corrections to be applied to the Euler equation without neglecting the spin-orbit current.

In symmetric nuclei, the spin-orbit potential W (9) reduces to the simpler form,

$$W = C_0^J J - C_0^{\nabla J} \nabla \rho. \tag{C1}$$

Injecting Eq. (C1) into Eq. (8) gives

$$J = B_J(\rho) \frac{\rho \nabla \rho}{f}, \tag{C2}$$

with

$$B_J(\rho) = \frac{2m}{\hbar^2} \frac{C_0^{\nabla J}}{1 + \frac{2m}{\hbar^2} C_0^J \frac{\rho}{f}}. \tag{C3}$$

Setting $C_0^J = 0$ in Eq. (C3) allows to recover the definition of the constant B_J used in this work. Now the coefficient B_J (C3) is a function of the density, and it will modify the Euler-Lagrange equation (12).

The correction to Eq. (13) induced by the spin-orbit current is given by the modification of only two terms:

$$C^{\nabla}(\rho) \to C^{\nabla}(\rho) + \frac{1}{2} C_0^{\nabla J} \frac{dB_J(\rho)}{d\rho} \frac{\rho}{f} \tag{C4}$$

$$\frac{dh}{d\rho} \to \frac{dh}{d\rho} - C_0^{J2} B_J(\rho) \frac{dB_J(\rho)}{d\rho} \rho. \tag{C5}$$

[1] M. Brack, C. Guet, and H. B. Hakansson, Phys. Rep. **123**, 275 (1985).
[2] J. Treiner and H. Krivine, Ann. Phys. (NY) **170**, 406 (1986).
[3] M. Centelles, M. Pi, X. Viñas, F. Garcias, and M. Barranco, Nucl. Phys. A **510**, 397 (1990).
[4] E. Surand and D. Vautherin, Phys. Lett. B **138**, 325 (1984).
[5] M. Pi, X. Viñas, M. Barranco, A. Perez-Canyellas, and A. Polls, Astron. & Astrophys. Suppl. Ser. **64**, 439 (1986).
[6] K. Washiyama, K. Bennaceur, B. Avez, M. Bender, P.-H. Heenen, and V. Hellemans, Phys. Rev. C **86**, 054309 (2012), and references. therein.
[7] M. Onsi, A. K. Dutta, H. Chatri, S. Goriely, N. Chamel, and J. M. Pearson, Phys. Rev. C **77**, 065805 (2008).
[8] A. Y. Potekhin, A. F. Fantina, N. Chamel, J. M. Pearson, and S. Goriely, Astron. Astrophys. **560**, A48 (2013).
[9] S. J. Lee and A. Z. Mekjian, Phys. Rev. C **82**, 064319 (2010).
[10] J. M. Lattimer and F. Douglas Swesty, Nucl. Phys. A **535**, 331 (1991).
[11] H. Shen, H. Toki, K. Oyamatsu, and K. Sumiyoshi, Prog. Theor. Phys. **100**, 1013 (1998).
[12] M. Hempel and J. Schaffner-Bielich, Nucl. Phys. A **837**, 210 (2010).
[13] N. Buyukcizmeci, A. S. Botvina, I. N. Mishustin, R. Ogul, M. Hempel, J. Schaffner-Bielich, F.-K. Thielemann, S. Furusawa, K. Sumiyoshi, S. Yamada, and H. Suzuki, Nucl. Phys. A **907**, 13 (2013).
[14] Shun Furusawa, Kohsuke Sumiyoshi, Shoichi Yamada, and Hideyuki Suzuki, ApJ, **772**, 95 (2013).
[15] Ad. R. Raduta and F. Gulminelli, Phys. Rev. C **82**, 065801 (2010).
[16] W. G. Newton and J. R. Stone, Phys. Rev. C **79**, 055801 (2009).
[17] E. Chabanat, P. Bonche, P. Haensel, J. Meyer, and R. Schaeffer, Nucl. Phys. A **635**, 231 (1998).
[18] P. Papakonstantinou, J. Margueron, F. Gulminelli, and Ad. R. Raduta, Phys. Rev. C **88**, 045805 (2013).
[19] A. Raduta, F. Gulminelli, and F. Aymard, Eur. Phys. J. A **50**, 24 (2014).
[20] W. D. Myers, W. J. Swiatecki, and C. S. Wong, Nucl. Phys. A **436**, 185 (1985).
[21] M. Bender, P.-H. Heenen, and P.-G. Reinhard, Rev. Mod. Phys. **75**, 121 (2003).
[22] J. Bartel, K. Bencheikh, and J. Meyer, Phys. Rev. C **77**, 024311 (2008).
[23] H. Krivine and J. Treiner, Phys. Lett. B **124**, 127 (1983).
[24] W. D. Myers and W. J. Swiatecki, Nucl. Phys. A **336**, 267 (1980).
[25] M. Centelles, M. D. Estal, and X. Vinas, Nucl. Phys. A **635**, 193 (1998).
[26] M. Warda, X. Vinas, X. Roca-Maza, and M. Centelles, Phys. Rev. C **80**, 024316 (2009).
[27] http://www.nndc.bnl.gov/amdc/
[28] P. Danielewicz and J. Lee, Nucl. Phys. A **818**, 36 (2009).
[29] Eur. Phys. J. A **20**(2) (2004), topical issue on nuclear symmetry energy, edited by B. A. Li, A. Ramos, G. Verde, and I. Vidana.
[30] P. Moller, W. D. Myers, H. Sagawa, and S. Yoshida, Phys. Rev. Lett. **108**, 052501 (2012).
[31] M. B. Tsang *et al.*, Phys. Rev. C **86**, 015803 (2012).
[32] P. Danielewicz, Nucl. Phys. A **727**, 233 (2003).
[33] P.-G. Reinhard, M. Bender, W. Nazarewicz, and T. Vertse, Phys. Rev. C **73**, 014309 (2006).
[34] N. Nikolov, N. Schunck, W. Nazarewicz, M. Bender, and J. Pei, Phys. Rev. C **83**, 034305 (2011).
[35] F. Douchin, P. Haensel, and J. Meyer, Nucl. Phys. A **665**, 419 (2000).
[36] M. Farine and J. M. Pearson, Phys. Lett. B **167**, 259 (1986).
[37] W. D. Myers and W. J. Swiatecki, Ann. Phys. (NY) **55**, 395 (1969).
[38] S. Typel, G. Röpke, T. Klahn, D. Blaschke, and H. H. Wolter, Phys. Rev. C **81**, 015803 (2010).
[39] G. Röpke, Phys. Rev. C **79**, 014002 (2009); Nucl. Phys. A **867**, 66 (2011).
[40] J. W. Negele and D. Vautherin, Nucl. Phys. A **207**, 298 (1973).
[41] P.-G. Reinhard and H. Flocard, Nucl. Phys. A **584**, 467 (1995).
[42] N. van Giai and H. Sagawa, Phys. Lett. B **106**, 379 (1981).
[43] L. G. Cao, U. Lombardo, C. W. Shen, and N. V. Giai, Phys. Rev. C **73**, 014313 (2006).
[44] H. Krivine and J. Treiner, J. Math. Phys. **22**, 2484 (1981).